Computational Forensic Analysis for the Chemical Weapons Attack at Khan Sheikhoun on April 4, 2017

Goong Chen[1,2,3], Cong Gu[1], Theodore A. Postol[4], Alexey Sergeev[1], Sanyang Liu[5], Pengfei Yao[6,7], and Marlan O. Scully[2,8,9]

[1]Department of Mathematics, Texas A&M University, College Station, TX 77843, USA
[2]Institute for Quantum Science and Engineering, Texas A&M University, College Station, TX 77843, USA
[3]School of Mathematics and Statistics, Xidian University Xi'an 710071, China, on sabbatical leave from Texas A&M University
[4]Program on Science, Technology, and National Security Policy (Emeritus), Massachusetts Institute of Technology, Cambridge, MA 02139, USA
[5]School of Mathematics and Statistics, Xidian University, Xi'an 710071, China
[6]Key Laboratory of Systems and Control, Institute of Systems Science, Academy of Mathematics and Systems Science, The Chinese Academy of Sciences, Beijing 100190, China
[7]School of Mathematical Sciences, University of Chinese Academy of Sciences, Beijing 100049, China
[8]Mechanical and Aerospace Engineering, Princeton University, Princeton, NJ 08544, USA
[9]Baylor Research and Innovation Collaborative, Baylor University, Waco, TX 76798, USA

Abstract

Advances in computational mathematics and mechanics provide a potentially powerful new forensic tool to reconstruct impacts, crashes and bombings, including those during military operations. This article applies these new tools to revisit the use of sarin gas or a similar chemical weapon on April 4, 2017 at Khan Sheikhoun in Idlib, Syria. Details of the attack are disputed; claims by the United States and the Organization for the Prohibition of Chemical Weapons–United Nations Joint Investigative Mechanism that the attack was carried out by the Syrian Air Force are contested by Syria and by Russia. To advance and clarify this debate, this article uses forensic computer simulations, including the LS-DYNA general purpose finite element analysis code from the Livermore Software Corporation, and 3D image analysis to model the crater that was identified as the source of the sarin release. Modeling of an artillery rocket and warhead, including the high explosives, and the paved road it struck suggests the observed crater and fragments could have been due to an improvised rocket-propelled artillery round with a high-explosive warhead. This calls into question the scenario of the attack described by the Joint Investigative Mechanism, which suggested that this crater was created by an aerial bomb and used that conclusion to assign the Syrian government responsibility for the chemical attack.

1 Introduction

One of the largest U.S. military operations in 2017 occurred on April 7, when the United States launched 59 Tomahawk cruise missiles from an Aegis cruiser, the USS Porter, against the Syrian government's airbase at Shayrat, Syria. This attack was aimed at punishing the Syrian Government for an alleged sarin nerve agent attack that had taken place seventy two hours earlier. The alleged attack took place on the morning of April 4, 2017 between 6 and 7 a.m. at Khan Sheikhoun (or, Khan Shaykhoun) in the Idlib Governorate of Syria. At the time the town was under the control of Tahrir al-Sham, previously known as the al-Qaeda affiliated al-Nusra Front. Press and social media reports based on information obtained from the local sources claimed that more than 80 people were killed and 500–600 people were injured.

The use of "sarin or a sarin-like substance" was later confirmed by the Organization for the Prohibition of Chemical Weapons (OPCW) Fact Finding Mission. Since the evidence examined by the mission included information and materials provided by the Syrian Government, the use of chemical weapons on that day is not questioned [1, p. 1]. Other details of the incident, however, have been in dispute. A summary of the U.S. Intelligence Community's assessment released on 11 April 2017 stated that the United States is confident that it was "a chemical weapon attack, using the nerve agent sarin," carried out by the Syrian Government [2]. The OPCW-UN Joint Investigative Mechanism (JIM) in its 26 October 2017 report also concluded that "the Syrian Arab Republic is responsible for the release of sarin at Khan Shaykhun on 4 April 2017" [3, para 46]. The Government of Syria disputed that finding and stated that no aircraft of the Syrian Air Force attacked Khan Sheikhoun at the time of the incident [3, para 42]. The Russian Government also questioned the JIM conclusions and criticized the methodology employed by the Mechanism. At the 16 November 2017 session of the UN Security Council Russia vetoed an extension of the Joint Investigative Mechanism's mandate when the Council did not support the proposal that Russia argued would strengthen the investigative protocols [4]. As a result, the conclusion about responsibility for the sarin attack in Khan Sheikhoun remains contested.

One of the reasons the doubts about the JIM conclusion and the earlier U.S. assessment persist is the lack of transparency regarding some of the key aspects of the investigations. The United States cited the need to protect sources and methods to justify withholding of the information that was used in the assessment. The JIM investigation presented more details about the incident, but did not fully explain the basis for reaching some of its key conclusions. The central piece of physical evidence that has been linked to the attack is a crater in the middle of an asphalt covered road in the northeast corner of Khan Sheikhoun. The White House intelligence report, the OPCW Fact-Finding Mission, and the JIM report point to this crater as the source of the sarin release. The JIM report further stated that "the crater had most likely been caused by a heavy object travelling at high velocity, such as an aerial bomb with a small explosive charge" [3, para 40]. In combination with the data about operations of the Syrian Air Force, this finding was used to support the conclusion about the chemical weapon release being a result of an air attack.

As noted earlier, none of the reports about the incident provide firm evidence in support of their claims about the origin of the crater. The JIM report stated that the Mechanism examined eight possible scenarios of the incident and conducted investigations into two of them - an aerial bomb and an improvised explosive device placed on the ground [3, para 38]. The analysis of the crater appears to have been limited to a review of photographs, videos and satellite images conducted by experts engaged by the Mechanism [3, para 40].

The objective of this paper is to provide an analysis that raises questions about the link between

the crater and an aerial bomb. The results of this analysis indicate that the crater that was identified as the source of a chemical release could have been generated by an improvised artillery rocket armed with a high-explosive warhead. It is not known if this scenario was among the eight examined by the JIM investigation and, if it was, on what basis it was excluded from detailed consideration. The JIM report cites opinions of experts who assessed that it is unlikely that the crater was created by a ground-launched weapon [3, Annex II, paras 50, 52]. However, this scenario was not discussed in detail and as the analysis presented in this paper demonstrates the evidence cited by the experts to support their conclusion does not in fact rule out the possibility of an artillery rocket explosion.

This paper examines the connections between evidence as observed at the scene and the physical sequence of events. It is done by means of computerized reconstruction and reenactment. This approach to event reconstruction is similar to that used in traditional forensic analyses of ballistics, except in this case we use advanced computational techniques to reconstruct the critical relevant features of the scene of the incident.

The organization of the paper is as follows:

(1) Section 2 considers the photographic evidence collected at the scene and selects images that show the crater at various points of time;

(2) Section 3 presents the results of detonation and impact simulations of a 122 mm rocket-propelled artillery explosion that shows that the cratering and projectile effects are consistent with the evidence observed at the scene. The crack pattern in the expended rocket motor casing indicates manufacturing defects that mean that the rocket was most likely made locally. These are done by the computer-modeling software LS-DYNA;

Concluding Remarks are given in Section 4. Concise technical details of the modeling and processing are deferred to Appendices I and II, especially the validation part.

Computer modeling, coding, supercomputing and visualization is a challenging activity, as each supercomputer run can easily take 3–5 days. Problems of such fast dynamics with detonation and destruction are well known to have high numerical instability and often tend to either diverge or produce physically inconsistent results. Fortunately, a prior paper [5] from the investigation of the rapid crash dynamics of the Germanwings Flight 9525, by incorporating the *FEA* (finite element analysis) and *SPH* (smooth particle hydrodynamics), has paved the foundation for validation and then the eventual success of the computational work presented here. Important *video animations* are included with their URLs and are *must-sees* for the reader in order to understand the underlying dynamics.

2 Photographic evidence

Since the attack occurred in a rebel-controlled zone, it was not accessible for inspection and evaluation by neutral parties (i.e., UN inspectors) due to the lack of guaranteed safe passage. Photographs of the crater provide the only available data for close examination.

The representative set of images of the crater was selected from the large number of images that were published in online media sources. The sources of the pictures and their sizes are listed in Table 2.1. The images are divided in two groups: (A) without a red skeletal marker, and (B) showing a rectangular red skeletal marker. In the latter group, the images show some signs of advanced disintegration of the crater along its border, see the comparisons below. This indicates that that the pictures in Group (B) were taken later than those in Group (A).

Image	Web address	Size (pixels)
A1	https://pbs.twimg.com/media/C8kEBpkXUAAXz1b.jpg	1200x800
A2	https://www.dr.dk/images/other/2017/04/08/scanpix-20170405-090310-1.jpg	3500x2333
A3	https://cdni.rt.com/russian/images/2017.08/original/59945338370f2ceb238b456e.jpg	1800x1000
A4	https://pbs.twimg.com/media/C-0fQqJXYAAfJmr.jpg	1136x852
B1	http://img.zeit.de/politik/ausland/2017-04/militaerschlag-syrien-donald-trump-giftgasanschlag-luftschlag-opposition-3/wide__1300x731	1300x731
B2	https://i1.wp.com/rfsmediaoffice.com/en/wp-content/uploads/2017/04/4032.jpg?ssl=1	1920x1152
B3	https://i.ytimg.com/vi/AqBqDzvtP-M/maxresdefault.jpg	1280x720

Table 2.1: Sources and sizes of the crater images to be analyzed.

The photographs show a metal fragment that resembles a shattered and bent pipe within it that could be the remnant of vessel that was the source of the sarin release and/or the munition that created the crater. The pipe is bent along its length and appears to be split open along a seam running parallel to its centerline. A number of other objects could be seen in the crater as well. However, the bent metal fragment is the only object that can be reliably linked to the crater as it is embedded into the ground unlike other fragments.

Comparison of the photographs from the two groups shows that the scene was modified at some point.

Pictures (A4) and (B2) were apparently taken from similar points of view and at the same time of day. This allows comparing them side-by-side; see Figure 2.1. The comparison shows that the border of the crater expanded in (B2) vs. (A4) by cracking, collapsing of pavement and chipping of crack edges. This advanced deterioration of the pavement indicates that the picture (B2) was taken at a later time. Considerable bending of the pipe on (B2) vs. (A4) as well as disappearance of loose debris on the pavement clearly shows that the site was modified after the image (A4) was taken.

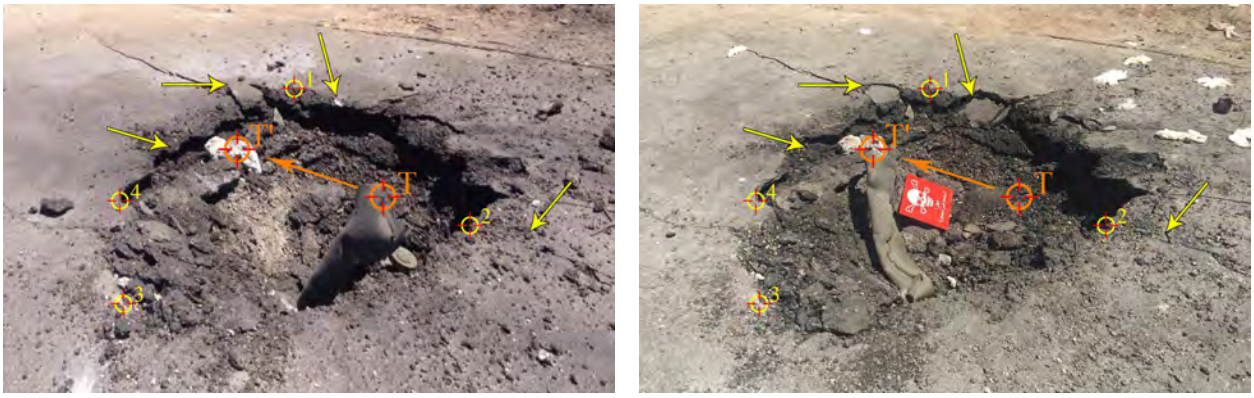

Figure 2.1: Comparison of the images (A4) (left panel) and (B2) (right panel). The observed differences in the crater shape are marked by yellow arrows. The orange arrow shows the bending direction of the pipe in image (B2). To make the comparison easier, the perspective of the image (A4) was slightly distorted (by approximately 10%) in order to make locations of four points (1–4) on the border of the crater exactly match in two images.

The most important change is the different bending directions of the top of the pipe: it points outward of the crater in (A4) and inward of the crater on (B2). Visual signs of modification are confirmed by a 3D image analysis, which is described in Appendix I.

The bending direction of the metal fragment plays an important role in the subsequent analysis.

The images of undisturbed site suggest that the twisted and broken pipe remnant was embedded at the forward edge of the crater during the impact process. The computer simulation described in the next section suggests that this could result from twisting of the metal motor casing along its length due to the sudden torque generated when the ground suddenly arrested the horizontal motion of the front of the casing while the rear was free to rotate forward.

3 Computational Forensics on Cratering from Computer Modeling with LS-DYNA

For the purposes of this analysis we followed the assumption made by Postol [6], who first observed and assessed that the metal fragment in the crater looks like a remnant of an improvised sarin dispenser made from a 122 mm artillery rocket. We hereby again closely examined the crater and the fragment and came to the same assessment. Unfortunately, due to the lack of access to the physical site that assumption cannot be positively confirmed. However, the results of the computer simulation presented here suggest that this assumption is consistent with the physical evidence from the site.

An improvised 122 mm artillery rocket would use an industrially produced high-explosive warhead. Common variants of these warheads weigh about 18 kg and have about 6.5 kg explosive charge. The exact weight of the charge in these easily purchased warheads varies somewhat but the explosive effects of charges of slightly different weights are essentially irrelevant to the findings shown in our calculations. Key parameters of the munition that was used in our computer simulations are given in Table 3.1.

The table also lists parameters of the impact that are based on the assumptions about the munition trajectory. Since the rocket motor casing (as seen in the photos of Section 2) is relatively small, we can assume that the rocket probably has a range of around 4–5 km. The angle at impact can have a range of 45°–70°.

To conduct simulation of the explosion we used the LS-DYNA tool [7], the chief commercialized product of computer modeling software made by the Livermore Software Corporation with more than forty-years history of development. Technical details of the simulation are provided in Appendix II. All the computations have been carried out on the ADA and Curie clusters at Texas A&M University's High Performance Computing Center. Each run took about three days or longer.

Parameter	Value
Total weight of rocket	27 kg
Weight of TNT H.E.	8.1 kg
Weight of warhead metal	10.1 kg
Terminal velocity	220 m/s
Angle	65°

Table 3.1: Parameters for the calculation of a 122 mm rocket warhead impact on an asphalt road.

We include Figure 3.1 with the sequence of six snapshots extracted from a video animation as the visualization output of our supercomputer results. The panels show the motion sequence, which leads to the end result of similarly what is observed in the photographs in the left column of Figure I.1. The frontal portion of the spent motor casing of the rocket is embedded in the soil near the

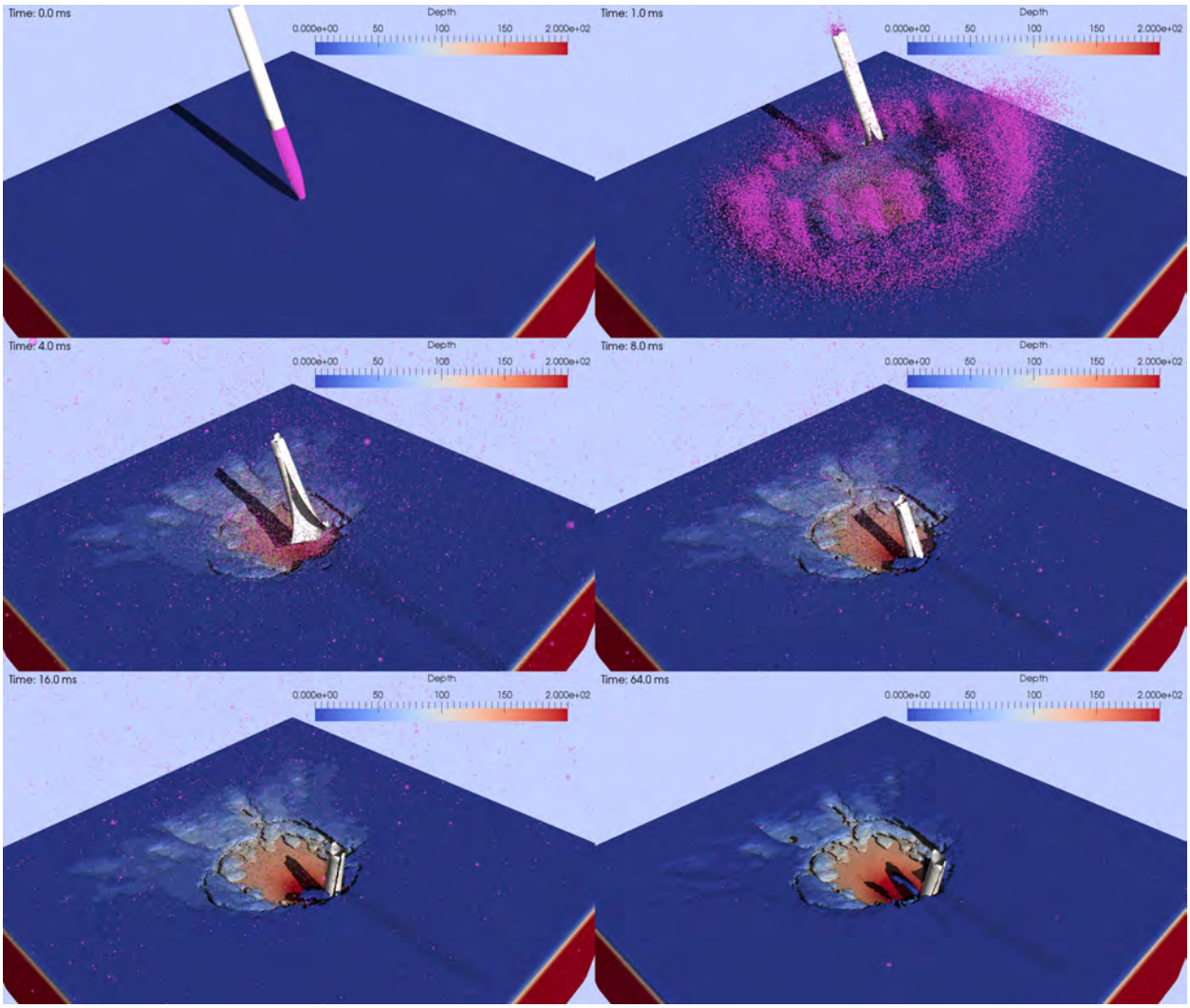

Figure 3.1: *This simulation contains the key assessment of this article.* The snapshots show the impact and explosion of a 122 mm artillery rocket. The rocket casing has manufacturing defects, causing a linear crack on a generatrix. The crater has a rough diameter of about 1.2 m and the remnant pipe has about 0.5 m above ground. The depth scale is in millimeters. For dynamic visualization, see the video in `https://www.dropbox.com/sh/mve31ivwl5tz0nx/AAAKMaXCqp0x-GaKEAYZ2g0Pa?dl=0&preview=BlastSR2-J5A-HD.mp4` .

edge of the crater, which matches the position of the metal fragment as seen on images that show the crater before it was modified. The fragment is slightly bent forward and is pointing outward by the sudden torque that occurs when the warhead impacts and then becomes lodged under the asphalt surface. If we assume that the rocket casing was fabricated into a pipe by welding, our calculations show similarly the kind of split or fissure along a generatrix of the pipe - the line on the cylinder parallel to its axis.

A close inspection of the back end of the embedded rocket motor casing shows an increase in the forward pointing curvature of the pipe and a fracture along the end-axis of the pipe from extreme

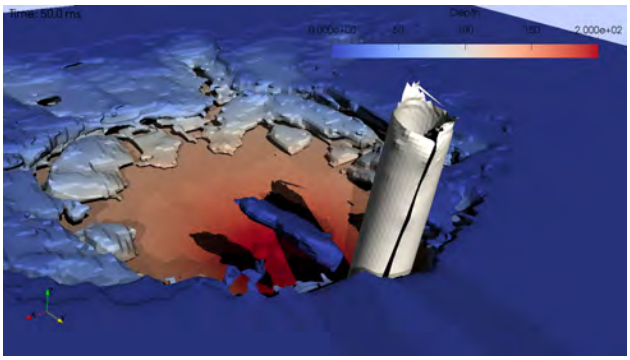

Figure 3.2: A zoomed-in view of the pipe in Figure 3.1.

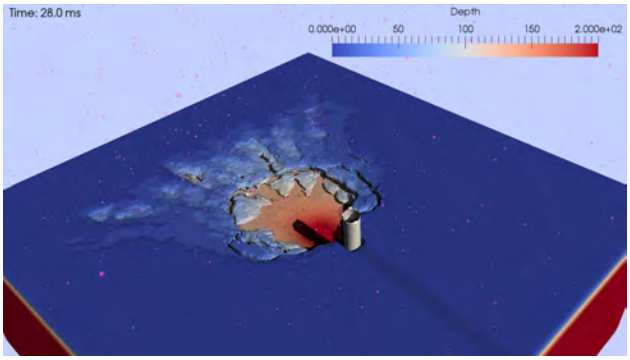

Figure 3.3: A snapshot of a 122 mm artillery rocket upon impact and explosion. This rocket is computed by using the same physical parameters as in Table 1, except that it does not have manufacturing defects. One sees no crack on the rocket casing. For dynamic visualization, see the video in `https://www.dropbox.com/sh/mve31ivwl5tz0nx/AAAKMaXCqp0x-GaKEAYZ2g0Pa?dl=0&preview=BlastSR2-J6A-HD.mp4`.

pulling forces. We believe that the extreme pulling forces that increased the curvature and caused the fracture of the rear pipe edge were the result of an attached nozzle and fin section being torn off during the extreme horizontal velocity deceleration at impact.

It is well known that cracks and fracture occur and propagate along the lines and locations where structural weakness and micro cracks preexist. The nearly linear crack split on the rocket motor casing (i.e., pipe) is due to the impact damage on the structure and then the propagation of the crack. The case computed in Figure 3.1 assumes the preexistence of structural weakness along a generatrix of the cylinder, due to possible welding in the fabrication of a pipe. The "line crack" can be seen in Figure 3.2 as a zoomed-in view of the pipe in Figure 3.1. We then have computed an additional case under exactly the same assumptions and with identical choices of parameters, but without any preexisting structural weakness on the pipe. The results show that the carcass then does not have a nearly linear crack; see Figure 3.3.

The arrival azimuth is easily identified because the rocket is embedded at the forward edge/side of the crater and the bent spent rocket casing also points forward along the direction of arrival. The cracking of the asphalt surface surrounding the crater, clearly visible with a radiative pattern, is due to hot gases propagating through the underlying ground and pushing the asphalt vertically.

We should emphasize that the calculations do not necessarily capture all possible inhomogeneities of the asphalt surface or of the ground underneath. Nevertheless, the computational mathematics and mechanics calculation essentially predicts most or all of the observed features of the crater at Khan Sheikhoun.

The Joint Investigative Mechanism appears to have looked into the scenario which assumed that the crater was produced by a "ground-launched" weapon or munition, although the report provides no details about specific assumptions made by the experts engaged by the JIM. Two separate arguments were made to exclude that scenario from consideration. First, it was stated that "no remnants peculiar to a rocket had been evident in the crater or found in its vicinity" [3, para 50]. This analysis, however, demonstrates that the metal fragment embedded in the crater could, in fact, be a remnant of an improvised rocket. It should be noted that no fragments characteristic of an aerial bomb, such as tail fins, were present at the site either. More importantly, since the access to the site was not restricted and, as we demonstrated earlier, it was modified after the crater was formed, the absence or, indeed, presence of fragments at the site that are not embedded in the ground cannot be used to support this conclusion in the JIM report.

Another argument made by the experts engaged by the JIM cites the scarcity of "visible signs of damage caused by fragmentation or overpressure, especially on the metal cabinet located 3 to 5 m away from the crater" [3, para 54]. Although it is not clear from the report, it appears that this observation applies to one of specific scenarios considered by the JIM, namely the one in which the crater was created by an explosive charge placed on the ground. In this scenario one indeed would expect to see a certain damage to the metal cabinet. However, in the scenario considered here, it should be taken into account that a cylindrical explosive charge, such as a 122-mm warhead considered in this analysis, would not produce a spherically-symmetrical blast wave or a debris cloud. For munitions with a high length-to-diameter ratio most debris would be distributed in an annular pattern that is perpendicular to the munition axis (pointed forward if the motion of the munition is taken into account). This effect, in fact, can be seen on the second panel of the explosion sequence shown on Figure 3.1. The location of the metal cabinet placed it in the solid angle that is unlikely to be affected by the explosion debris.

It therefore can be stated with substantial confidence that the observed crater is consistent with the impact of an improvised rocket that used a standard 122 mm explosive warhead. If that is the case, the munition that created the crater could not have been used as a sarin delivery device, since in the model considered in this analysis, the volume of the improvised rocket would be used up by the propellant and the explosive warhead. The split pipe that the JIM report identified as evidence of a container filled with sarin is simply the casing of the rocket motor that propelled the warhead to the location of the explosion.

4 Concluding Remarks

This paper demonstrated the use of a powerful new forensic tool based on computational mathematics and mechanics that allowed us to model characteristics of the munition that was used in the attack on the civilian population of Khan Sheikhoun on the morning of April 4, 2017. We have shown that the crater that the OPCW Fact Finding Mission and the UN-OPCW Joint Investigative Mechanism identified as the most likely point of release of sarin used in the attack is consistent with the result of an explosion of an improvised artillery rocket armed with a small explosive warhead. This calls into question the conclusions of the Joint Investigative Mechanism and

of the earlier White House report that linked the chemical weapons attack in Khan Sheikhoun to an aerial bomb. Since that link was an important factor in attributing the use of chemical weapons to an attack by the Syrian Air Force, it also raises questions about that attribution. An analysis of various scenarios of the incident, however, is beyond the scope of this article.

It is extremely important that the international community holds accountable the perpetrators of chemical attacks. For this to happen, it is essential to have an established investigation mechanism that could conduct impartial investigation of all incidents of alleged use of chemical weapons. It is also essential to ensure that these investigations are based on scientifically sound analysis and that that they are conducted in a transparent way. The investigation of the April 4, 2017 incident in Khan Sheikhoun illustrates this point. In considering the formation of the crater that is believed to be at the source of the sarin release the investigation was based exclusively on a visual examination of photo and video evidence. The methodology used by the experts engaged by the Joint Investigative Mechanism to reach their conclusions was never explained. As the analysis presented in this paper demonstrates, there are scenarios of an incident that are consistent with the observed evidence that would call into question the key conclusions of the JIM report regarding the origin of the crater and potentially about the attribution of the attack.

Regrettably, the termination of the UN-OPCW Joint Investigative Mechanism mandate in November 2017 appears to have ended further attempts to investigate the incident in Khan Sheikhoun. We hope that this analysis will contribute to establishing of facts of that incident and will help reliably identify the perpetrators of the chemical attack in Khan Sheikhoun.

Acknowledgement

S. Liu is partially supported by The National Natural Science Foundation of China Grant No. 61373174. P. Yao is partially supported by The National Natural Science Foundation of China Grants No. 61473126 and No. 61573342, and Key Research Program of Frontier Sciences, CAS, No. QYZDJ-SSW-SYS011. M.O. Scully is partially supported by The Robert A. Welch Foundation Grant No. A-1261. We thank Texas A&M University's High Performance Computing Center for the generous allocation of supercomputing hours on the Ada and Curie cluster.

References

[1] *REPORT OF THE OPCW FACT-FINDING MISSION IN SYRIA REGARDING AN ALLEGED INCIDENT IN KHAN SHAYKHUN, SYRIAN ARAB REPUBLIC APRIL 2017.* June 2017. URL: `https://www.opcw.org/fileadmin/OPCW/Fact_Finding_Mission/s-1510-2017_e_.pdf` (visited on 08/01/2018).

[2] *The Assad Regime's Use of Chemical Weapons on April 4, 2017.* Apr. 2017. URL: `https://assets.documentcloud.org/documents/3553049/Syria-Chemical-Weapons-Report-White-House.pdf` (visited on 08/01/2018).

[3] *Seventh report of the Organisation for the Prohibition of Chemical Weapons-United Nations Joint Investigative Mechanism.* Oct. 2017. URL: `https://www.securitycouncilreport.org/atf/cf/%7B65BFCF9B-6D27-4E9C-8CD3-CF6E4FF96FF9%7D/s_2017_904.pdf` (visited on 08/01/2018).

[4] Security Council Meetings Coverage. *Security Council Fails to Adopt 2 Draft Resolutions on Extending Mandate of Joint Mechanism Investigating Chemical Weapons Attacks in Syria*. Nov. 16, 2017. URL: https://www.un.org/press/en/2017/sc13072.doc.htm (visited on 01/08/2018).

[5] G. Chen, Y.-C. Wang, A. Perronnet, C. Gu, P. Yao, B. Bin-Mohsin, H. Hajaiej, and M. O. Scully. "The advanced role of computational mechanics and visualization in science and technology: analysis of the Germanwings Flight 9525 crash". In: *Physica Scripta* 92.3 (2017), p. 033002.

[6] T. A. Postol. *A Quick Turnaround Assessment of the White House Intelligence Report Issued on April 11, 2017 About the Nerve Agent Attack in Khan Shaykhun, Syria*. URL: https://d.ibtimes.co.uk/en/file/99/postol-report-1.pdf (visited on 11/02/2017).

[7] *LS-DYNA*. Livermore Software Technology Company. URL: http://www.lstc.com/products/ls-dyna.

[8] Y. Ma, S. Soatto, J. Kosecka, and S. S. Sastry. *An Invitation to 3-D Vision: From Images to Geometric Models*. Vol. 26. Springer Science & Business Media, 2012.

[9] R. Hartley and A. Zisserman. *Multiple View Geometry in Computer Vision*. Cambridge university press, 2003.

[10] J. Wu, L. Li, X. Du, and X. Liu. "Numerical study on the asphalt concrete structure for blast and impact load using the Karagozian and case concrete model". In: *Applied Sciences* 7.2 (2017), p. 202.

[11] E. L. Fasanella, K. H. Lyle, and K. E. Jackson. *Developing soil models for dynamic impact simulations*. 2009. URL: https://ntrs.nasa.gov/search.jsp?R=20090022374.

[12] J. Strange, C. Denzel, and T. McLane III. *Cratering from High Explosive Charges. Analysis of Crater Data*. Tech. rep. Army Engineer Waterways Experiment Station, Vicksburg, MS, 1961.

Appendix I Corresponding Points, Epipolar Geometry and the Fundamental Matrix

I.1 Movement of Bent Pipe Evidencing Changes to the Original Crater

This Appendix presents the results of a 3D image analysis based on calculation of the so called *fundamental matrix* between images (A1)/(B1), as well as between (A1)/(B2) and (A1)/(B3). As discussed in the paper, visible signs of crater degradation prove that the images in Group A were taken earlier than those in Group B. We create the epipolar lines in the image (A1) that correspond to the location of the tip of the pipe in the images from Group (B). The intersection of epipolar lines shows the location of the tip of the pipe in the images from Group (B) as it would be seen in the image (A1). Figure I.2 shows that the pipe has been bent in the images from Group (B) from outward to inward of the crater.

From a mathematical point of view, an image is a projective mapping of a three-dimensional object into a plane. Since two different images of the same object may be results of different projections, their comparison is not straightforward. However, locations of a given physical point in two different images are closely related. Introducing *homogeneous coordinates* $\mathbf{x} \equiv (x, y, 1)$, as

Figure I.1: Eight corresponding points (1–8) in images (A1), (B1), (A2), (B2), (A3), and (B3). The point (T) marks the tip of the pipe.

in *projective geometry*, of a point (x, y) in the first image and $\mathbf{x}' \equiv (x', y', 1)$ of the corresponding point (x', y') in the second image, this relationship can be expressed as the linear constraint [8, 9]

$$\mathbf{x}'^{\mathrm{T}} \mathsf{F} \mathbf{x} = 0. \tag{1}$$

The matrix F in (1) is called the *fundamental matrix*. It depends only on internal parameters of the cameras and their positions. If the location of a point in the second image, $\mathbf{x}'$, is known, then

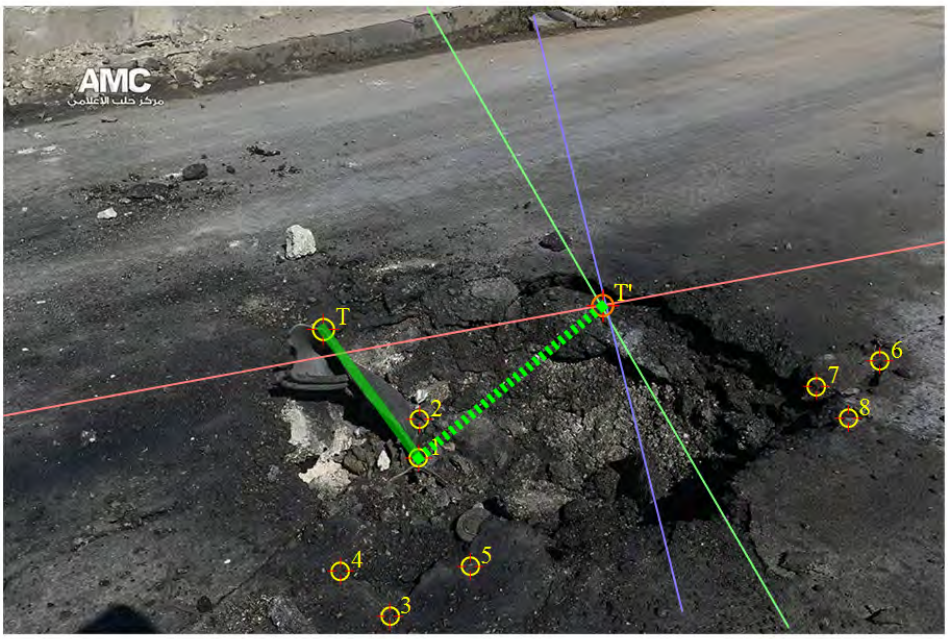

Figure I.2: The scene in image (A1) with epipolar lines showing re-projection of the tip of the (T) from the images of Group (B) into the image (A1), red, green and blue lines for (B1), (B2), and (B3) images, respectively. Red circle at their intersection shows the tip from Group (B) as it would be seen in image (A1), as a point (T'). Bold green line connects points (1) and (T) and shows direction of the pipe in Group (A), while the dashed line does in Group (B).

possible locations of the same point in the first image, $\mathbf{x}$, may be anywhere on the line defined by (1). This line is known as *epipolar line*.

Our first task is calculating the fundamental matrix between two images using a set of *eight* pairs of corresponding points. We write down a set of eight homogeneous equations

$$\mathbf{x'}^{(n)^{\mathrm{T}}} \mathsf{F} \mathbf{x}^{(n)} = 0, \tag{2}$$

for each pair of corresponding points $\left(\mathbf{x'}^{(n)}, \mathbf{x}^{(n)}\right)$, $n = 1, \ldots 8$. Since F is 3×3 matrix with 8 unknown elements (we could always set $F_{11} = 1$ because of homogeneity of the equations), 8 equations are generally sufficient to resolve the linear system for 8 unknowns.

The corresponding points of the images were selected manually as some prominent "landmark" points that are clearly visible in each photo and that are associated with solid and unmovable physical objects. Our choice of corresponding points is shown in Figure I.1.

Appendix II LS-DYNA Computer Modeling of Explosion and Impact; Validation

Modeling and computation of the problem under consideration require fundamental mathematical models like partial differential equations for *aerodynamics (hot gas), solid dynamics (paved road),*

fracture mechanics, explosion dynamics, and their interactions. By proper set-up, LS-DYNA is able to take all of them into account. This Appendix provides the foundation for modeling and computation methodologies for Section 3.

LS-DYNA is a general purpose finite element analysis software developed by LSTC [7]. It has accumulated numerous capabilities and functions that are powerful in simulating complex real-world transient dynamic problems such as crash and explosion. We have successfully used LS-DYNA for the study just as in that for the pulverizing crash of Germanwings Flight 9525 [5], where it is found that a combination of *Finite Element Analysis* (FEA) and *Smoothed Particle Hydrodynamics* (SPH) can yield excellent results.

The problem of asphalt pavement under blast and impact load has been studied numerically using LS-DYNA by other researchers; see [10], for example. In the current study, we use solid elements to model the paved road, shell elements to model the structure of the artillery rocket, and SPH particles to model the warhead including the high explosives. The process of the explosion and impact of the artillery rocket, consisting of a warhead and a motor pipe behind, can be described as follows. The warhead explodes upon contact with the road, creating damage. The motor part then keeps moving downward and crashes into the ground. The basic spatial setup of the simulation is shown in Figure II.1. Details of the modeling of each component are discussed below.

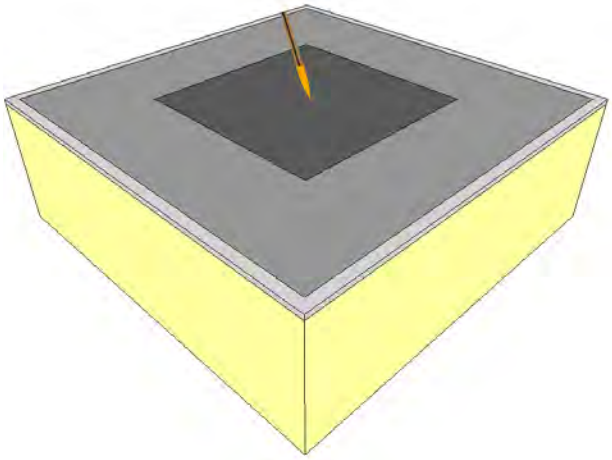

Figure II.1: Overview of simulated parts.

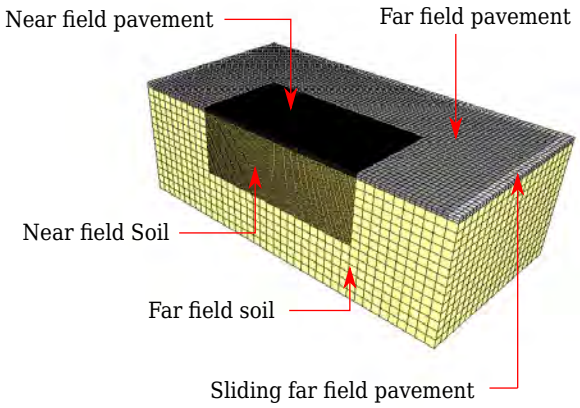

Figure II.2: Section of paved ground model.

II.1 Modeling of Paved Road

The road is modeled as an asphalt pavement of 10 cm in thickness, and a soil foundation underneath. The pavement consists of three parts, the *near field*, the *far field* (coarse grids) and the *sliding far field*. The sliding far field is tied to the soil underneath, but its tangential sliding is permitted. The soil is also modeled with a near field part and a far field part with a different grid size. See Figure II.2 for a cross-section of the ground. The material model for the asphalt chosen in LS-DYNA is `MAT_CONCRETE_DAMAGE_REL3` with parameter generation, while the material model for the soil is `MAT_SOIL_AND_FOAM`. Major material parameters are shown in Table II.1.

Parameter	Value
Density of asphalt	2320 kg/m^3
Unconfined compression strength of asphalt	4.6 MPa
Strain rate effect for asphalt	[10, Figure 6]
Maximum principal strain at erosion for asphalt	0.08
Minimum principal strain at erosion for asphalt	-0.08
Density of soil	2100 kg/m^3
Shear modulus of soil	60 MPa
Yield coefficients of soil	[11, Table 2]
Compressibility of soil	[11, Figure 14]

Table II.1: Material parameters for the paved road.

II.2 Modeling an Artillery Rocket

The artillery rocket consists of a warhead and a motor. The warhead has a metal casing with high explosives inside. They are both modeled with SPH. The motor pipe has a longitudinal *structural weakness intended to signify a welding seam*, and is modeled by collocated nodes tied with `CONSTRAINED_TIE-BREAK`. There is a strengthened edge (larger thickness) along the seam of the structural weakness. See Figure II.3. The material model of high explosive is `MAT_HIGH_EXPLOSIVE_BURN`. The important equation of state of high explosives is `EOS_JWL` (the empirical *Jones-Wilkins-Lee equation of state*), given by

$$p = A\left(1 - \frac{\omega}{R_1 V}\right) e^{-R_1 V} + B\left(1 - \frac{\omega}{R_2 V}\right) e^{-R_2 V} + \frac{\omega E}{V}.$$

The material model for steel is `MAT_PLASTIC_KINEMATIC`, whose strain rate effect is accounted for by the *Cowper-Symonds model*

$$\frac{\sigma_y}{\sigma_0} = 1 + \left(\frac{\dot{\varepsilon}}{C}\right)^{1/p}.$$

Major parameters are listed in Tables II.2 and II.3.

II.3 Contact Modeling

Contact settings are summarized in Table II.4. *Erosion* is enabled for the pavement to simulate damage and perforation. The motor pipe has a "tie on contact" type of contact with the soil, which is meant to simulate the fixation of the motor pipe in the ground after having lodged into the soil. Static frictional coefficient is set to be 0.8 and dynamic frictional coefficient is set to be 0.6 where applicable.

II.4 Validation of SPH Blast Simulation

Validation is a crucial, indispensable part of any computational mechanics study. The computed data must be validated against those from experiments. Artillery rocket explosion damage data are hard (or, nearly impossible) to come by. Therefore, we validated our explosion data versus the

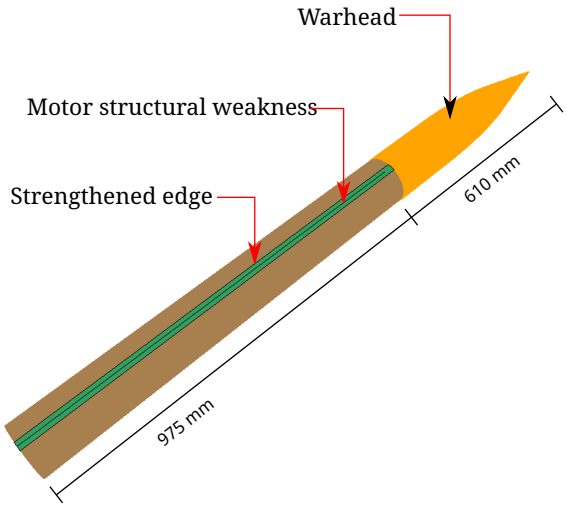

Figure II.3: Schematic of an artillery rocket.

Parameter	Value
Density	1630 kg/m^3
Detonation velocity	6930 m/s
Chapman-Jouget pressure	21 GPa
A in JWL	371.2 GPa
B in JWL	2.23 GPa
R_1 in JWL	4.15
R_2 in JWL	0.95
ω in JWL	0.3
Initial E in JWL	7 GJ/m^3
Initial V in JWL	1.0

Table II.2: Parameters for high explosive (TNT).

crater formation data from high-explosive blasts collected by the U.S. Army Corps of Engineers [12].

In this validation, we use Smoothed Particle Hydrodynamics (SPH) to simulate buried, contact ($0 < \lambda_c < 0.053$), and near field ($0.053 < \lambda_c < 0.4$) blast load, where λ_c is the reduced charge position with unit m/kg$^{1/3}$. In our situation, $\lambda_c \approx 0.12$ if the warhead is detonated upon ground impact with a 45° landing angle.

In our validation simulation, we set up a ball-shaped 5 lb TNT charge at various locations above the soil. The shear modulus of soil is lowered to 20 MPa, from 60 MPa in Table II.1, which is meant to model a stronger gravel rich mixture. In Figures II.4(a) and (b), craters in our simulation are compared with the cratering data collected by the U.S. Army Corps of Engineers [12]. The data manifest that they lie well within the range of experiments.

Parameter	Value
Density of Steel	7800 kg/m^3
Young's modulus	200 GPa
Poisson's ratio	0.29
Yield stress	310 MPa
Tangent modulus	1 Gpa
Kinematic hardening parameter	0.3
C in Cowper-Symonds model	40 s^{-1}
p in Cowper-Symonds model	5
Effective plastic strain at erosion	0.7
Motor thickness	3 mm
Motor edge thickness	5 mm
Warhead casing thickness	6 mm

Table II.3: Parameters for rocket steel parts.

Slave	Master	Contact
Warhead	Pavement	`ERODING_NODES_TO_SURFACE`
Warhead	Other	`AUTOMATIC_NODES_TO_SURFACE`
Motor	Pavement	`ERODING_SURFACE_TO_SURFACE`
Motor	Soil	`AUTOMATIC_SURFACE_TO_SURFACE_TIEBREAK` (Option 1 – tie on contact)
Sliding far field pavement	Soil	`AUTOMATIC_SURFACE_TO_SURFACE_TIEBREAK` (Option 4 – slide)
Near field pavement	Far field pavement	`TIED_NODES_TO_SURFACE`
Near field soil	Far field soil	`TIED_NODES_TO_SURFACE`
Other	–	`AUTOMATIC_SINGLE_SURFACE`

Table II.4: Contact settings.

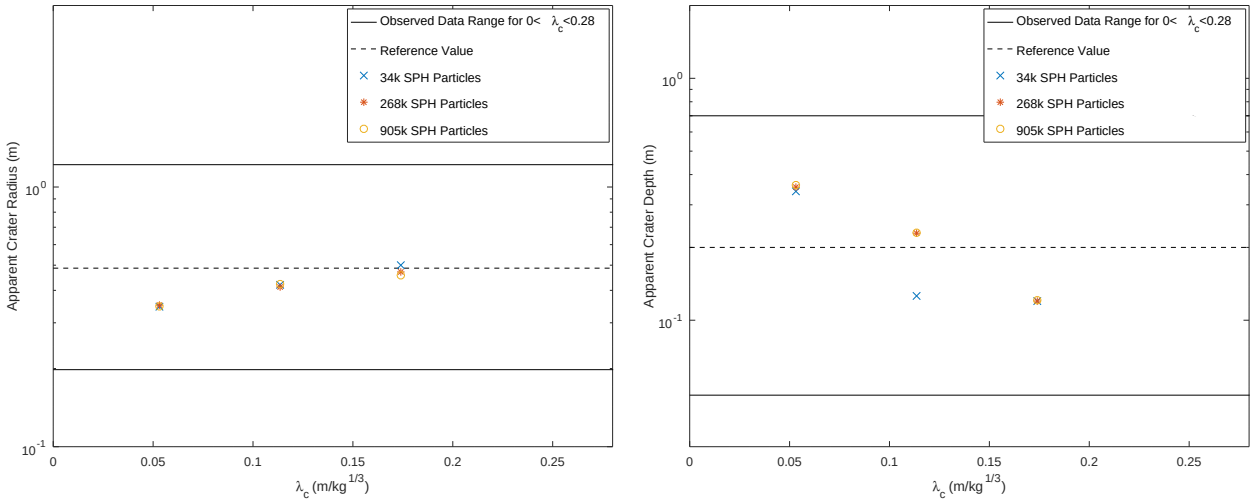

Figure II.4: Ball-shaped, 5 lb TNT charge detonated at various locations above the soil. Comparison of (a) apparent crater radius, and (b) apparent crater depth with [12].

II.5 Modeling of Bomb-Detonation-on-the-Ground Scenarios

We used the technique to examine other potential scenarios of the crater formation. Postol [6] earlier suggested a blast configuration as shown in Figure II.5. The outcome of the blast shows a totally different damaged and fractured pipe than the one seen in the crater, Figures 2.1–I.2. See also the associated video animation link in the caption of Figure II.5.

Setting up the pipe and high-explosive stick in different configurations, as given in Figures II.6 and II.7, only produces outcomes of a damaged and fractured pipe which look similar to that in Figure II.5(b). Therefore, this scenario was dismissed.

Figure II.5: (a) A possible configuration first proposed by Postol [6]; (b) A snapshot where one can see a totally different fracture pattern of the pipe. Thus, this configuration has been disproved. Video in `https://www.dropbox.com/sh/mve31ivwl5tz0nx/AAAKMaXCqp0x-GaKEAYZ2g0Pa?dl=0&preview=BlastSEC2-HD.mp4`.

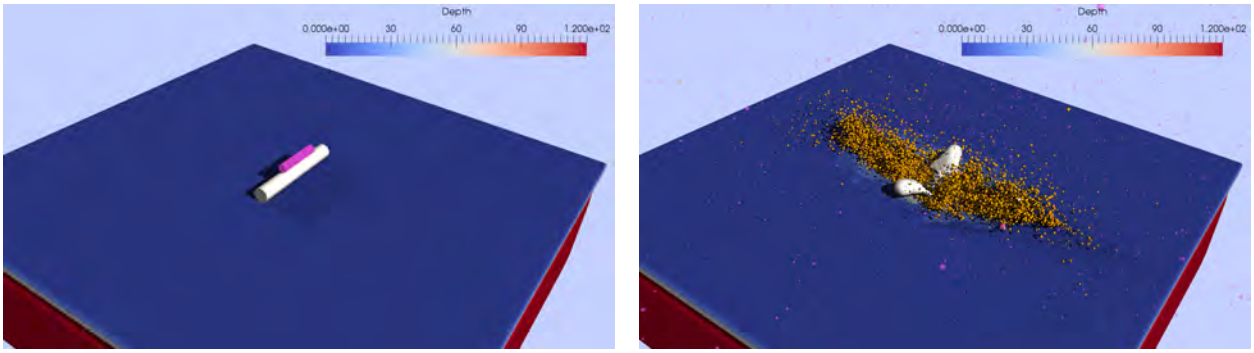

(a) (b)

Figure II.6: This layout between the explosive (on top) and the pipe is different from that in Figure II.5. However, the fracture pattern of the pipe is similar, which is different from the pipe on the crater site so it is again dismissed. Video in `https://www.dropbox.com/sh/mve31ivwl5tz0nx/AAAKMaXCqp0x-GaKEAYZ2g0Pa?dl=0&preview=BlastSEC3-HD.mp4` .

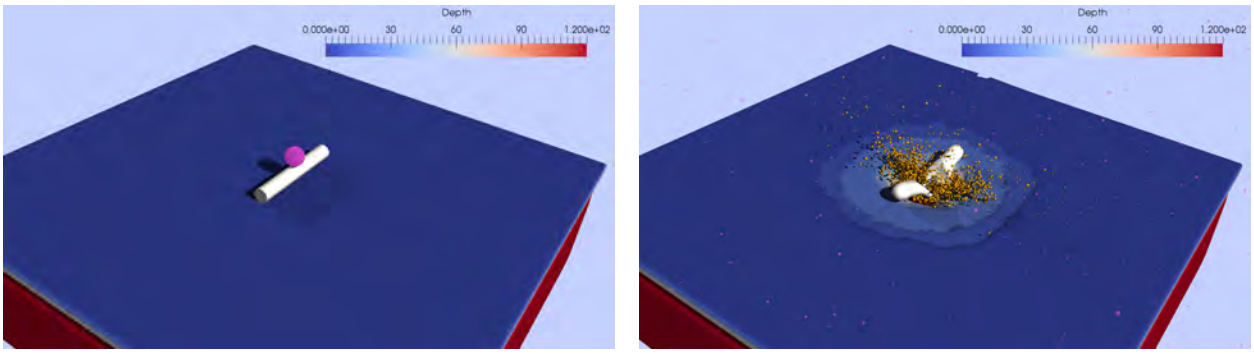

(a) (b)

Figure II.7: Here the explosive is spherical. Again, the eventual crack pattern in (b) leads to its dismissal. Video in `https://www.dropbox.com/sh/mve31ivwl5tz0nx/AAAKMaXCqp0x-GaKEAYZ2g0Pa?dl=0&preview=BlastSEC4-HD.mp4` .